Heliyon 10 (2024) e30908

Contents lists available at ScienceDirect

Heliyon

journal homepage: www.cell.com/heliyon

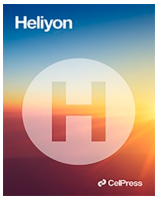

Research article

Pharmacological inhibition of p300 ameliorates steatosis, inflammation, and fibrosis in mice with non-alcoholic steatohepatitis

Jung-Yeon Kim [a,1], Ah Young Yang [a,1], Kiryeong Kim [b], Hyun Hee Kwon [b], Jaechan Leem [a,*], Yun-A Kim [c,**]

[a] Department of Immunology, School of Medicine, Daegu Catholic University, Daegu, Republic of Korea
[b] Department of Internal Medicine, School of Medicine, Daegu Catholic University, Daegu, Republic of Korea
[c] Department of Family Medicine, School of Medicine, Daegu Catholic University, Daegu, Republic of Korea

ARTICLE INFO

Keywords:
Non-alcoholic steatohepatitis
p300
Inflammation
Fibrosis
Ferroptosis
Endoplasmic reticulum stress

ABSTRACT

The histone acetyltransferase p300 plays a pivotal role in regulating gene expression and cellular phenotype through epigenetic mechanisms. It significantly influences lipid metabolism, which is a key factor in the pathogenesis of non-alcoholic steatohepatitis (NASH), by modulating the transcription of genes involved in lipid synthesis and accumulation. This study aimed to investigate the protective potential of inhibiting p300 in NASH. Male C57BL/6J mice were subjected to a methionine- and choline-deficient (MCD) diet for 4 weeks to induce NASH, and during this period, the p300 inhibitor C646 (10 mg/kg) was administered three times a week. C646 treatment reduced the elevation of p300 expression and histone H3 acetylation, leading to a decrease in liver injury markers in the serum and an improvement in the histological abnormalities observed in MCD diet-fed mice. C646 also reduced lipid accumulation by modulating de novo lipogenesis and suppressed inflammation, including cytokine overproduction and macrophage infiltration. Furthermore, C646 mitigated liver fibrosis and myofibroblast accumulation. This protective effect was achieved through the inhibition of apoptosis by reducing p53 and Bax expression and the suppression of ferroptosis by decreasing lipid peroxidation while enhancing antioxidant defenses. Additionally, C646 alleviated endoplasmic reticulum stress, as evidenced by the downregulation of unfolded protein response signaling molecules. These results highlight the potential of p300 as a therapeutic target for NASH.

1. Introduction

Non-alcoholic fatty liver disease (NAFLD) stands as the most prevalent form of chronic liver disease globally, affecting approximately 25 % of the adults [1]. NAFLD encompasses a range of conditions, from simple steatosis to the more severe non-alcoholic steatohepatitis (NASH). While simple steatosis typically follows a benign course, NASH, occurring in 20–30 % of NAFLD patients,

* Corresponding author.
** Corresponding author.
E-mail addresses: jcim@cu.ac.kr (J. Leem), yakim@cu.ac.kr (Y.-A. Kim).
[1] These authors equally contributed to this work.

https://doi.org/10.1016/j.heliyon.2024.e30908
Received 19 December 2023; Received in revised form 7 May 2024; Accepted 7 May 2024
Available online 9 May 2024

can progress to cirrhosis and liver cancer [1]. The underlying cellular and molecular mechanisms are not yet fully elucidated, but the "multi-hit" hypothesis is widely accepted as an explanation for the pathogenesis of NASH. This hypothesis postulates that the transition from simple steatosis to NASH involves multiple contributing factors, including genetic and epigenetic factors, insulin resistance, adipokines, nutritional influences, and the gut microbiota [2,3]. Currently, NASH ranks as the second leading cause of liver transplantation and imposes a significant economic burden on a global scale [1]. Unfortunately, there are presently no approved pharmaceutical treatments for NASH, underscoring the urgent need for the development of effective interventions with substantial clinical implications.

Epigenetics offers a promising perspective for understanding the pathophysiology of NAFLD, as it has the capacity to influence gene expression without causing alterations to the DNA sequence [4]. Lifestyle factors such as weight gain and lack of physical activity have been shown to impact the pathogenesis of NAFLD through epigenetic mechanisms [4]. Epigenetic changes intricately participate in modulating multiple processes such as lipid metabolism, insulin sensitivity, mitochondrial function, and redox balance, all of which are relevant to the pathophysiology of NAFLD [4,5]. Because epigenetic modifications are reversible, they offer a flexible interface between an individual and their environment, making them attractive targets for therapeutic interventions [6]. These epigenetic modifications encompass histone modifications, DNA methylation, and non-coding RNAs. Posttranslational modifications of histones, such as acetylation, methylation, and phosphorylation of histone tails, regulate chromatin structure and gene expression [7]. Among them, acetylation is one of the most extensively studied. Histone acetylation is controlled by the opposing functions of histone acetyltransferases and histone deacetylases [7]. Within the family of histone acetyltransferases, p300 plays a pivotal role in multiple cellular processes, including apoptosis, proliferation, and differentiation, by regulating histone acetylation-dependent chromatin compactness and accessibility [8]. Lines of evidence suggests that abnormal p300 expression contributes to the pathophysiology of cancers [8], cognitive and neurodegenerative diseases [9], and cardiovascular diseases [10]. Recently, we demonstrated that the administration of garcinol, a natural p300 inhibitor, can ameliorate cisplatin-evoked nephrotoxicity in mice by effectively restraining oxidative stress, inflammation, and apoptosis [11]. Peng et al. have also reported that pharmacological suppression of p300 can inhibit lipopolysaccharide-induced cytokine production in macrophages and alleviate acute liver injury in mice [12]. Moreover, emerging evidence points to p300's involvement in hepatic lipid metabolism, gluconeogenesis, and inflammatory responses [13,14]. Kim et al. have even demonstrated the anti-fibrotic action of p300 inhibition in two mouse models of liver fibrosis evoked by choline-deficient high-fat diet or by thioacetamide [15]. Nevertheless, a comprehensive understanding of the exact function of p300 in the pathophysiology of NASH is still lacking. The purpose of this study is to investigate the effects of pharmacologically inhibiting p300 on the key aspects of NASH, such as steatosis, inflammation, and fibrosis. Our investigation focuses on the role of C646, a potent and selective inhibitor of the p300 enzyme, in a methionine- and choline-deficient (MCD) diet-induced model of NASH. This particular model is extensively used and recognized in the field for its ability to effectively replicate the pathogenesis of NASH and assess potential therapeutic agents [16,17]. By conducting this study, we aim to contribute significant insights into the viability of targeting p300 as a therapeutic strategy for mitigating the symptoms of NASH, thus addressing a crucial gap in the current array of treatment options.

2. Materials and methods

2.1. Animal experiments

Six-week old male C57BL/6J mice were procured from HyoSung Science (Daegu, Korea). All the mice were accommodated in an environment with ambient temperatures ranging from 20 to 24 °C, maintained on a 12/12-h light/dark cycle, and provided with unrestricted access to both water and food. The experimental protocol received approval from the Institutional Animal Care and Use Committee of the Daegu Catholic University Medical Center (DCIAFCR-220628-10-Y). Following a one-week acclimatization period, all the mice were randomly divided into three groups (n = 8 for each group): Control, MCD, and MCD + C646 groups. The Control group was provided with a standard chow diet, while both the MCD and MCD + C646 groups were fed the MCD diet for a duration of four weeks. These diets were obtained from Dyets (Bethlehem, PA, USA) and their composition has been described in detail in previous literature [18]. In the case of the MCD + C646 group, mic were intraperitoneally administered C646 (10 mg/kg; Selleckchem, Houston, TX, USA; Fig. 1) every other day, three times a week, throughout the period in which they were fed the MCD diet. We prepared the C646 injection solution by first dissolving it in dimethyl sulfoxide (DMSO) to create a stock solution, which was then diluted with phosphate-buffered saline (PBS) to achieve the desired 10 mg/kg concentration. The final concentration of DMSO in the injection solution was 5 % (*v*/*v*). On the other hand, mice in both the Control and MCD groups were intraperitoneally injected with an equivalent

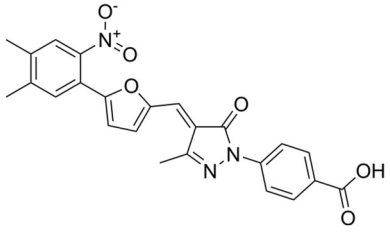

Fig. 1. Chemical structure of C646.

volume of the vehicle, which was 5 % DMSO solution in PBS, during the same time frame. The dosage of C646 was determined in accordance with prior studies [19,20]. The body weight of the mice was monitored on a weekly basis during the entire duration of the experiment. At the end of the experiment, all the mice were euthanized and their cardiac puncture was performed for blood sample collection, while their liver tissues were weighed and collected for subsequent analysis.

2.2. Biochemical analysis

Serum aspartate aminotransferase (AST) and alanine aminotransferase (ALT) levels were measured using an automatic analyzer (Hitachi, Osaka, Japan). Hepatic triglyceride (TG) levels were quantified using the triglyceride assay kit (Abcam, Cambridge, MA, USA). The concentrations of tumor necrosis factor-α (TNF-α), interleukin-6 (IL-6), IL-1β, and chemokine (C–C motif) ligand 2 (CCL2) in the serum were determined through the use of ELISA kits (R&D Systems, Minneapolis, MN, USA). The assessment of hepatic malonaldehyde (MDA) concentrations was carried out using the MDA assay kit (Sigma-Aldrich), while hepatic glutathione (GSH) levels were analyzed with the GSH detection kit (Enzo Life Sciences, Farmingdale, NY, USA). All assays adhered to the manufacturers' recommended protocols.

2.3. Hematoxylin and eosin (H&E), Masson's trichrome, and oil red O staining

The liver tissues were promptly fixed in a 4 % paraformaldehyde solution and subsequently embedded in paraffin. These paraffin-embedded tissue blocks were sectioned and mounted on glass slides. The slides were stained with H&E or Masson's trichrome and examined using a 3DHISTECH Pannoramic MIDI slide scanner (Budapest, Hungary). The assessment of liver injury severity was based on the NAFLD activity score [21], a semi-quantitative measure used to categorize each case in terms of steatosis (0–3), lobular inflammation (0–3), or hepatocellular ballooning (0–2), with evaluations performed across 5 randomly selected fields at 200 × magnification for each sample. For oil red O staining, frozen liver sections were rapidly fixed in 4 % paraformaldehyde. Following this, the cytoplasm's lipid droplets were stained using an oil red O solution (Sigma-Aldrich), while the nuclei were counterstained with hematoxylin. The percentage of the area stained with oil red O or Masson's trichrome was quantified using i-Solution DT software from 5 randomly selected fields (400 × magnification for oil red O and 200 × magnification for Masson's trichome) for each sample.

2.4. Immunohistochemistry (IHC) and terminal deoxynucleotidyl transferase dUTP nick end labeling (TUNEL) staining

For IHC, liver sections (4 μm thick) embedded in paraffin were first deparaffinized using xylene. They were then rehydrated gradually through a series of ethanol solutions. Antigen retrieval was performed by incubating the sections in Epitope Retrieval Solution 2 (EDTA-buffer, pH 8.8) at 98 °C for 20 min. The sections were washed and subsequently treated with 3 % hydrogen peroxide in methanol for 10 min to inhibit endogenous peroxidase activity. After additional washing, the sections were incubated for 1 h at 37 °C with primary antibodies diluted at 1:100. The primary antibodies used included anti-p300 (Santa Cruz Biotechnology, Dallas, TX, USA), anti-F4/80 (Santa Cruz Biotechnology), anti-α-smooth muscle actin (α-SMA; Sigma-Aldrich), and anti-4-hydroxynonenal (4-HNE; Abcam). Detection was achieved using the EnVision System (DAKO, Agilent, Santa Clara, CA, USA) for 30 min at 37 °C. The staining process involved 3,30-diaminobenzidine tetrahydrochloride as the chromogen and hematoxylin as the counterstain. Slides were then scanned with a 3DHISTECH Pannoramic MIDI slide scanner. Quantification of the areas stained with p300, α-SMA, or 4-HNE was performed in 5 random fields at 200 × magnification for each sample, and the number of F4/80-positive cells was counted in 5 random fields at 400 × magnification for each sample.

Apoptosis was detected using a TUNEL assay kit (Roche Diagnostics, Indianapolis, IN, USA) following the manufacturer's instructions. Liver sections were deparaffinized, rehydrated, and permeabilized in 10 mM Tris-HCl (pH 7.4) for 30 min at room temperature. After washing, the sections were incubated with the TUNEL reaction mixture for 1 h at 37 °C. Nuclei were counterstained with DAPI. Images were captured using a Nikon confocal microscope (Tokyo, Japan). Positive cells were identified and counted in 5 random fields at 600 × magnification for each sample.

2.5. Western blot analysis

The extraction of total proteins was carried out by first treating liver tissue samples with a lysis buffer. After the proteins were successfully extracted, they were loaded onto poly-acrylamide gels. Subsequently, these loaded proteins were transferred to nitrocellulose membranes. The membranes were incubated with primary antibodies targeting specific proteins, including acetyl-histone H3 (Lys18; Cell Signaling Technology, Danvers, MA, USA), acetyl-histone H3 (Lys9; Cell Signaling Technology), histone H3 (Cell Signaling Technology), p-NFκB p65 (Cell Signaling Technology), NFκB p65 (Cell Signaling Technology), fibronectin (Abcam), vimentin (Cell Signaling Technology), transforming growth factor-β1 (TGF-β1; R&D Systems), α-SMA (Sigma-Aldrich), p53 (Cell Signaling Technology), Bax (Santa Cruz Bio-technology), NADPH oxidase 4 (NOX4; Novus Biologicals, Littleton, CO, USA), actyl-CoA synthetase long chain family member 4 (ACSL4; Santa Cruz Bio-technology), glutathione peroxidase 4 (GPX4; Abcam), xCT (Proteintech, Rosement, IL, USA), activating transcription factor 6 (ATF6; Abcam), p-eukaryotic initiation factor 2α (p-eIF2α; Cell Signaling Technology), eIF2α (Cell Signaling Technology), CCAAT/enhancer-binding protein homologous protein (CHOP; Thermo Fisher Scientific, Waltham, MA, USA), or glyceraldehyde-3-phosphate dehydrogenase (GAPDH; Cell Signaling Technology). Following primary antibody incubation, the membranes underwent a washing step and subsequently subjected to secondary antibody probing. Protein bands were then visualized through the application of enhanced chemiluminescence reagents (Thermo Fisher Scientific) and quantified using the

ImageJ software.

2.6. Real-time quantitative reverse transcription-polymerase chain reaction (qRT-PCR)

Total RNA was extracted from liver tissue samples using the TRIzol reagent (Sigma-Aldrich). The reverse transcription reaction was conducted with the PrimeScript RT Reagent Kit (TaKaRa, Tokyo, Japan) according to the manufacturer's instructions. PCR mixtures were prepared containing 100 ng of cDNA and 100 pM each of forward and reverse primers. The amplification process involved an initial denaturation step at 95 °C for 10 min, followed by 45 cycles. Each cycle consisted of denaturation at 95 °C for 20 s, annealing at 60 °C for 30 s, and extension at 72 °C for 20 s. Real-time PCR was carried out using the Power SYBR Green PCR Master Mix (Thermo Fisher Scientific) in the Thermal Cycler Dice Real Time System III (TaKaRa). The primers utilized for this process are detailed in Table 1. For the quantification of relative gene expression, the $2-^{\Delta\Delta CT}$ method was applied, using GAPDH as the internal control for normalization.

2.7. Statistical analysis

The data are presented as the mean ± SD and analyzed using GraphPad Prism 6.07 software. To ensure appropriate analysis, the Shapiro-Wilk normality test was first conducted to assess the distribution of the data. For normally distributed data, one-way ANOVA with Tukey's HSD *post hoc* test was used. In cases of non-normal distribution, the Kruskal-Wallis test with Dunn's *post hoc* test was applied. Additionally, for comparative analyses involving body weight across different groups and time points, two-way ANOVA with Tukey's HSD *post hoc* test was utilized. Values of $p < 0.05$ were considered statistically significant.

Table 1
List of primers.

Gene	Primer sequence (5'→3')	Accession No.
SREBP-1c	F: ACGGAGCCATGGATTGCACA R: AAGGGTGCAGGTGTCACCTT	NM_001358314
ACC1	F: GAATCTCCTGGTGACAATGCTTATT R: GGTCTTGCTGAGTTGGGTTAGCT	NM_133360
FASN	F: CTGAGATCCCAGCACTTCTTGA R: GCCTCCGAAGCCAAATGAG	NM_007988
ChREBP	F: CCCTCAGACACCCACATCTT R: CAGAGCTCAGAAAGGGGTTG	NM_021455
TNF-α	F: ACTTCGGGGTGATCGGTCCCC R: TGGTTTGCTACGACGTGGGCTAC	NM_013693
IL-6	F: TACCACTTCACAAGTCGGAGGC R: CTGCAAGTGCATCATCGTTGTTC	NM_031168
IL-1β	F: TGCAGCTGGAGAGTGTGGATCCC R: TGTGCTCTGCTTGTGAGGTGCTG	NM_008361
CCL2	F: GGGCCTGCTGTTCACAGTT R: CCAGCCTACTCATTGGGAT	NM_011333
COL1A1	F: AGCACGTCTGGTTTGGAGAG R: GACATTAGGCGCAGGAAGGT	NM_007742
COL3A1	F: CGTAAGCACTGGTGGACAGA R: TCTGAGGAATGCCAGCTGCA	NM_009930
Fibronectin	F: GCAGTGACCACCATTCCTG R: GGTAGCCAGTGAGCTGAACAC	NM_001276410
Vimentin	F: GATCGATGTGGACGTTTCCAA R: GTTGGCAGCCTCAGAGAGGT	NM_011701
α-SMAa	F: CCACCGCAAATGCTTCTAAGT R: GGCAGGAATGATTTGGAAAGG	NM_007392
GRP78	F: CTGAGGCGTATTTGGGAAAGAA R: TGACATTCAGTCCAGCAATAGTG	NM_001163434
IRE1α	F: GGTCCAATCGTACGGCAGTT R: TCTCTCACAGAGCCACCTTTGTAG	NM_023913
Perk	F: AGCACTCAGATGGAGAGAGTCAG R: GCTATGGGAGTTGTTGGACTGT	NM_004836
ATF4	F: GAGCTTCCTGAACAGCGAAGTG R: TGGCCACCTCCAGATAGTCATC	NM_009716
ATF6	F: CCCAAGCTCTCCGCATAGTC R: CAGGAACGTGCTGAGTTGAA	NM_001081304
CHOP	F: CCTAGCTTGGCTGACAGAGG R: CTGCTCCTTCTCCTTCATGC	NM_007837
GAPDH	F: TGGAAAGCTGTGGCGTGAT R: TGCTTCACCACCTTCTTGAT	NM_001289726

3. Results

3.1. C646 inhibits p300-dependent histone acetylation and alleviates liver injury in MCD diet-fed mice

We initially assessed the expression levels of p300 in the liver across all groups. IHC staining using an anti-p300 antibody showed that mice fed the MCD diet had significantly higher hepatic p300 expression compared to controls ($p < 0.001$; Fig. 2A and B). Furthermore, feeding with the MCD diet resulted in increased acetylation levels of Lys18 and Lys9 on histone H3 in the liver ($p < 0.001$ for Lys18, $p < 0.01$ for Lys9; Fig. 2C and D), suggesting enhanced p300 activity. However, treatment with C646 notably reduced both the p300 expression ($p < 0.001$; Fig. 2A and B) and the acetylation levels of these lysine residues on histone H3 ($p < 0.001$ for Lys18, $p < 0.01$ for Lys9; Fig. 2C and D), indicating its efficacy in modulating p300-related pathways in NASH induced by the MCD diet.

Parameters such as body weight, liver weight, and liver/body weight ratio decreased after feeding with the MCD diet ($p < 0.001$ for all; Fig. 3A, B, C). C646 treatment did not significantly affect these parameters (Fig. 3A, B, C). H&E staining of liver tissues displayed typical histological features of NASH in MCD diet-fed mice, including macrovesicular steatosis, hepatocellular ballooning, and inflammatory cell infiltration (Fig. 3D). However, these changes were largely reversed by C646 (Fig. 3D). In line with these findings, the increase in the NAFLD activity score in mice fed the MCD diet was effectively mitigated by C646 ($p < 0.001$; Fig. 3E). To evaluate the extent of liver injury, serum AST and ALT levels were measured. Feeding with the MCD diet led to a marked increase in both liver injury markers, but C646 treatment effectively reduced the liver damage caused by the MCD diet ($p < 0.001$ for both; Fig. 3F and G).

3.2. C646 reduces hepatic lipid accumulation in MCD diet-fed mice

To evaluate the impact of C646 on hepatic lipid accumulation, we conducted oil red O staining on liver sections. The percentage of the area stained with oil red O was significantly increased in MCD diet-fed mice ($p < 0.001$; Fig. 4A and B). C646 treatment markedly decreased the extent of oil red O staining ($p < 0.001$; Fig. 4A and B). Biochemical assessment of hepatic TG content further corroborated the anti-steatotic effect of C646 ($p < 0.01$; Fig. 4C). We next examined the influence of C646 on the expression of lipogenesis-related genes such as sterol regulatory element binding protein-1c (SREBP-1c), acetyl-coenzyme A carboxylase 1 (ACC1), fatty acid synthase (FASN), and carbohydrate-responsive element-binding protein (ChREBP) in the liver. Our findings revealed that C646 treatment significantly decreased the mRNA expression of SREBP-1c, ACC1, FASN, and ChREBP in MCD diet-fed mice ($p < 0.001$ for SREBP-1c, $p < 0.001$ for ACC1, $p < 0.01$ for FASN, $p < 0.01$ for ChREBP; Fig. 4D).

3.3. C646 alleviates liver inflammation in MCD diet-fed mice

To evaluate the impact of C646 on liver inflammation, we measured the concentrations of cytokines in the serum. Feeding with the MCD diet increased serum levels of TNF-α, IL-6, IL-1β, and CCL2 ($p < 0.001$ for all; Fig. 5A). C646 treatment effectively decreased the

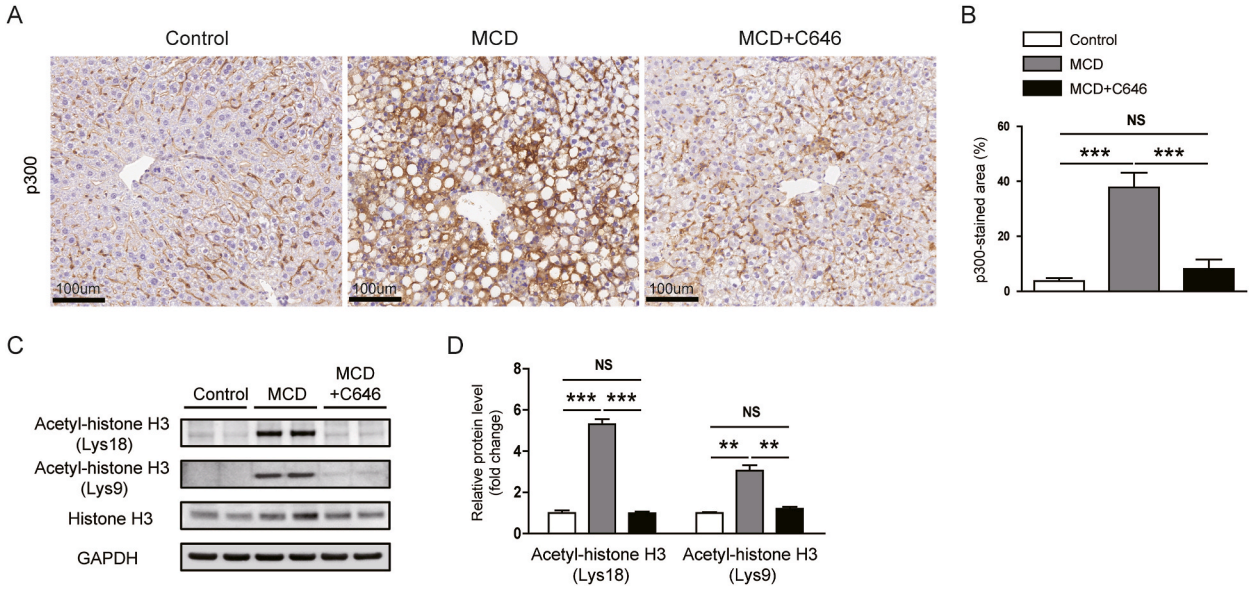

Fig. 2. Impact of C646 on p300 expression and histone H3 acetylation in MCD diet-fed mice. (A) IHC staining of liver tissues for p300. Scale bar = 100 μm. (B) Percentage of areas displaying p300 staining (one-way ANOVA with Tukey's HSD *post hoc* test, n = 8). (C) Western blots depicting acetyl-histone H3 (Lys18) and acetyl-histone H3 (Lys9) in liver tissues. The uncropped versions of Western blots are shown in Supplementary of Original Images for Blots. (D) Quantitative analysis of Western blot data (Kruskal-Wallis test with Dunn's *post hoc* test, n = 6). Data are expressed as the mean ± SD. $^{**}p < 0.01$ and $^{***}p < 0.001$. NS, not significant.

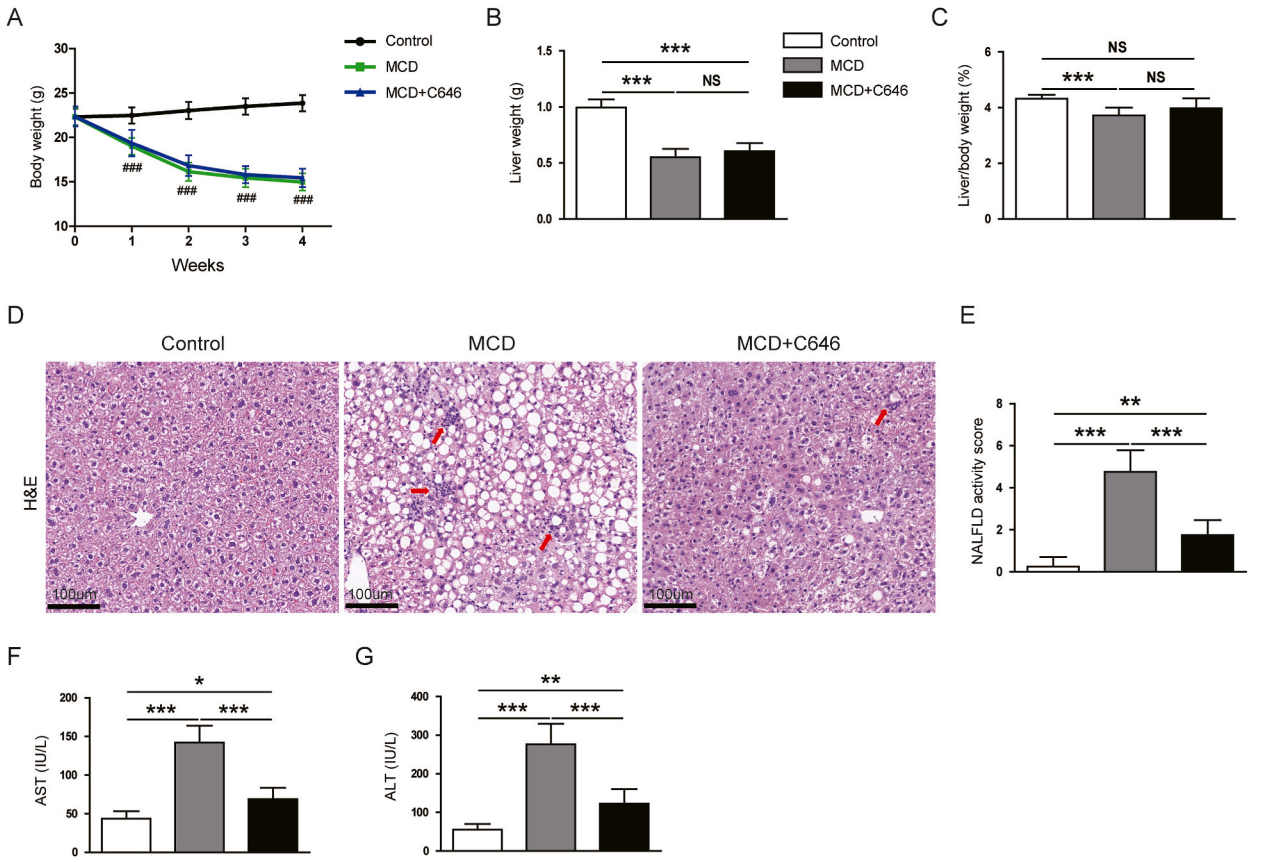

Fig. 3. Improvement of liver injury by C646 in MCD diet-fed mice. (A) Monitoring of mouse body weight during the feeding period (two-way ANOVA with Tukey's HSD *post hoc* test, n = 8). $^{###}p < 0.001$ compared to the control group. There was no significant difference between the MCD group and the MCD + C646 group. (B) Measurement of liver weight (one-way ANOVA with Tukey's HSD *post hoc* test, n = 8). (C) Calculation of the liver-to-body weight ratio (one-way ANOVA with Tukey's HSD *post hoc* test, n = 8). (D) H&E staining of liver tissues. The red arrows indicate inflammatory cell infiltration. Scale bar = 100 μm. (E) Assessment of NAFLD activity scores (Kruskal-Wallis test with Dunn's *post hoc* test, n = 8). (F) Serum levels of AST (one-way ANOVA with Tukey's HSD *post hoc* test, n = 8). (G) Serum levels of ALT (one-way ANOVA with Tukey's HSD *post hoc* test, n = 8). Data are expressed as the mean ± SD. $^{*}p < 0.05$, $^{**}p < 0.01$ and $^{***}p < 0.001$. NS, not significant.

levels of these cytokines ($p < 0.001$ for TNF-α, $p < 0.001$ for IL-6, $p < 0.01$ for IL-1β, $p < 0.01$ for CCL2; Fig. 5A). Additionally, hepatic mRNA levels of TNF-α, IL-6, IL-1β, and CCL2 were markedly decreased by C646 ($p < 0.001$ for all; Fig. 5B). IHC staining using an antibody against F4/80, a pan-macrophage marker, on liver sections demonstrated a significant reduction in the number of F4/80-positive macrophages in MCD diet-fed mice with C646 treatment ($p < 0.001$; Fig. 5C and D). We subsequently examined the effect of C646 on NFκB activation, and the results showed that C646 effectively suppressed the phosphorylation of NFκB p65 in MCD diet-fed mice ($p < 0.05$; Fig. 5E and F).

3.4. C646 mitigates liver fibrosis and attenuates myofibroblast accumulation in MCD diet-fed mice

Masson's trichrome staining of liver tissues demonstrated a significant reduction in the area of positive staining for collagen fibers in MCD diet-fed mice following C646 treatment ($p < 0.001$; Fig. 6A and B). Increased mRNA levels of collagen type I alpha 1 (ColA1), collagen type III alpha 1 (Col3A1), fibronectin, and vimentin in mice exposed to the MCD diet were markedly reduced by C646 treatment ($p < 0.001$ for all; Fig. 6C). Western blot analysis further confirmed the inhibitory effect of C646 on the protein levels of fibronectin, vimentin and TGF-β1 in MCD diet-fed mice ($p < 0.01$ for fibronectin, $p < 0.05$ for vimentin, $p < 0.05$ for TGF-β1; Fig. 6D and E). These findings indicate that p300 inhibition effectively mitigates liver fibrosis in MCD diet-fed mice.

To assess the impact of C646 on myofibroblast accumulation, we measured the expression levels of α-SMA, a well-established marker for myofibroblasts, in the liver. As expected, feeding with the MCD diet increased hepatic mRNA expression of α-SMA ($p < 0.001$; Fig. 7A). C646 treatment significantly reduced the mRNA expression of α-SMA ($p < 0.001$; Fig. 7A). The increase in α-SMA protein levels in mice exposed to the MCD diet was also mitigated by C646 treatment ($p < 0.05$; Fig. 7B and C). IHC staining with an anti-α-SMA antibody further validated that C646 treatment attenuated α-SMA expression in mice exposed to the MCD diet ($p < 0.001$; Fig. 7D and E).

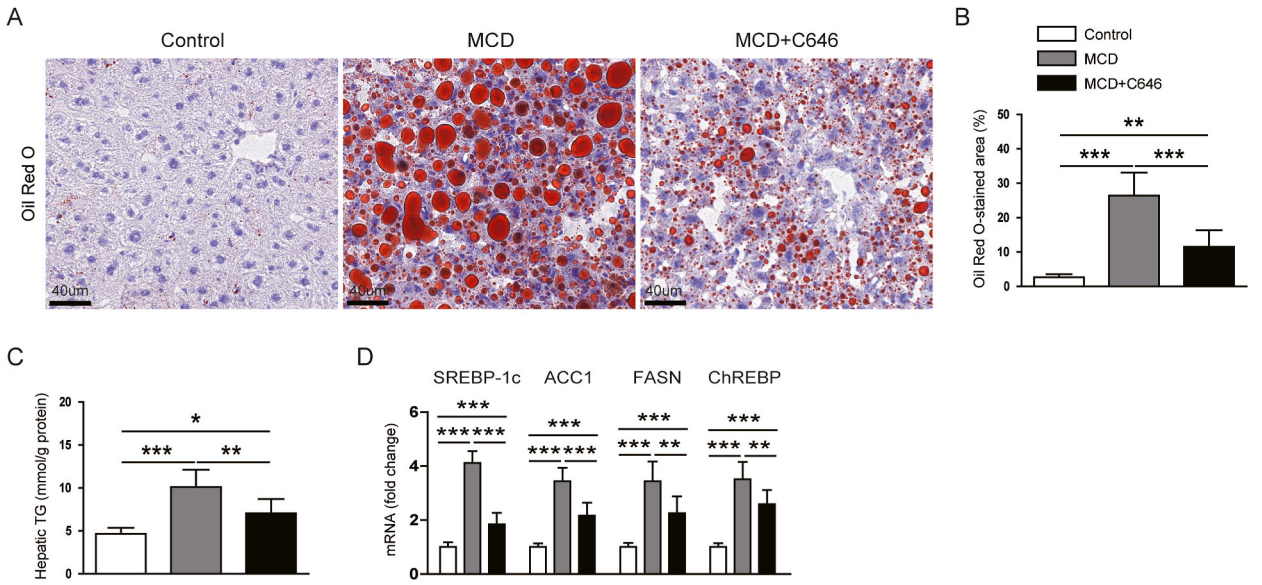

Fig. 4. C646 mitigates hepatic lipid accumulation in MCD diet-fed mice. (A) Oil red O staining of liver tissues. Scale bar = 40 μm. (B) Percentage of areas with oil red O staining (one-way ANOVA with Tukey's HSD *post hoc* test, n = 8). (C) TG content in liver tissues (one-way ANOVA with Tukey's HSD *post hoc* test, n = 8). (D) mRNA expression of SREBP-1c, ACC1, FASN, and ChREBP in liver tissues (one-way ANOVA with Tukey's HSD *post hoc* test, n = 8). Data are expressed as the mean ± SD. $^{*}p < 0.05$, $^{**}p < 0.01$ and $^{***}p < 0.001$.

3.5. C646 prevents apoptosis and ferroptosis in MCD diet-fed mice

To investigate the impact of C646 on hepatocyte apoptosis, we conducted TUNEL assay on liver sections. As expected, mice fed the MCD diet had a significant increase in the number of TUNEL-stained cells compared to controls ($p < 0.001$; Fig. 8A and B). C646 treatment effectively inhibited hepatocyte apoptosis ($p < 0.001$; Fig. 8A and B). Elevated protein expression of p53 and Bax in mice exposed to the MCD diet was also decreased by C646 ($p < 0.05$ for both; Fig. 8C and D).

To determine whether C646 could inhibit ferroptosis in MCD diet-evoked NASH, we first assessed lipid peroxidation in the liver. IHC staining of 4-HNE, a lipid peroxidation product, showed increased hepatic expression levels of 4-HNE after feeding with the MCD diet ($p < 0.001$; Fig. 9A and B), whereas C646 remarkably decreased 4-HNE expression levels in MCD diet-fed mice ($p < 0.001$; Fig. 9A and B). Hepatic levels of MDA, another lipid peroxidation product, were also considerably increased after feeding with the MCD diet ($p < 0.001$; Fig. 9C). C646 treatment effectively reduced MDA levels in MCD diet-fed mice ($p < 0.001$; Fig. 9C). Additionally, the increased expression of the prooxidant enzyme NOX4 in mice fed the MCD diet was remarkably reduced by C646 ($p < 0.01$; Fig. 9D and E). C646 treatment also effectively attenuated the increase in protein expression of ACSL4, which is essential for ferroptosis induction, in MCD diet-fed mice ($p < 0.05$; Fig. 9D and E). Protein levels of the antioxidant enzyme GPX4 were higher in mice fed the MCD diet than in controls ($p < 0.05$; Fig. 9D and E). Interestingly, C646 treatment enhanced GPX4 expression in MCD diet-fed mice ($p < 0.05$; Fig. 9D and E). In addition, while mice exposed to the MCD diet exhibited lower hepatic levels of the cystine/glutamate antiporter xCT compared to controls, C646 significantly restored xCT expression in MCD diet-fed mice ($p < 0.05$; Fig. 9F and G). Consistent with these findings, the decreased GSH levels in mice fed the MCD diet were also significantly restored by C646 ($p < 0.01$; Fig. 9H).

3.6. C646 suppresses endoplasmic reticulum (ER) stress in MCD diet-fed mice

To investigate the effects of C646 on ER stress signaling pathways in MCD diet-evoked NASH, we assessed the expression of ER stress markers in the liver. Feeding with the MCD diet led to elevated mRNA expression of glucose-regulated protein 78 (GRP78), inositol-requiring enzyme 1α (IRE1α), protein kinase RNA-like ER kinase (PERK), ATF4, ATF6, and CHOP ($p < 0.001$ for all; Fig. 10A). C646 treatment remarkably downregulated the expression of these markers ($p < 0.001$ for GRP78, $p < 0.01$ for IRE1α, $p < 0.01$ for PERK, $p < 0.001$ for ATF4, $p < 0.001$ for ATF6, $p < 0.001$ for CHOP; Fig. 10A). Furthermore, the increased protein levels of ATF6, p-eIF2α, and CHOP in mice exposed to the MCD diet were notably reduced by C646 ($p < 0.05$ for ATF6, $p < 0.05$ for p-eIF2α, $p < 0.01$ for CHOP; Fig. 10B and C). These results suggest that p300 inhibition mitigates ER stress signaling pathways in MCD diet-induced NASH.

4. Discussion

In addressing the pathophysiology of NASH, it is essential to understand the role of gene modulation as a foundational step. NASH is characterized by an intricate interplay of genetic, metabolic, and environmental factors [2,3]. At the genetic level, alterations in gene expression play a pivotal role in initiating and advancing the disease. This modulation is largely driven by epigenetic mechanisms,

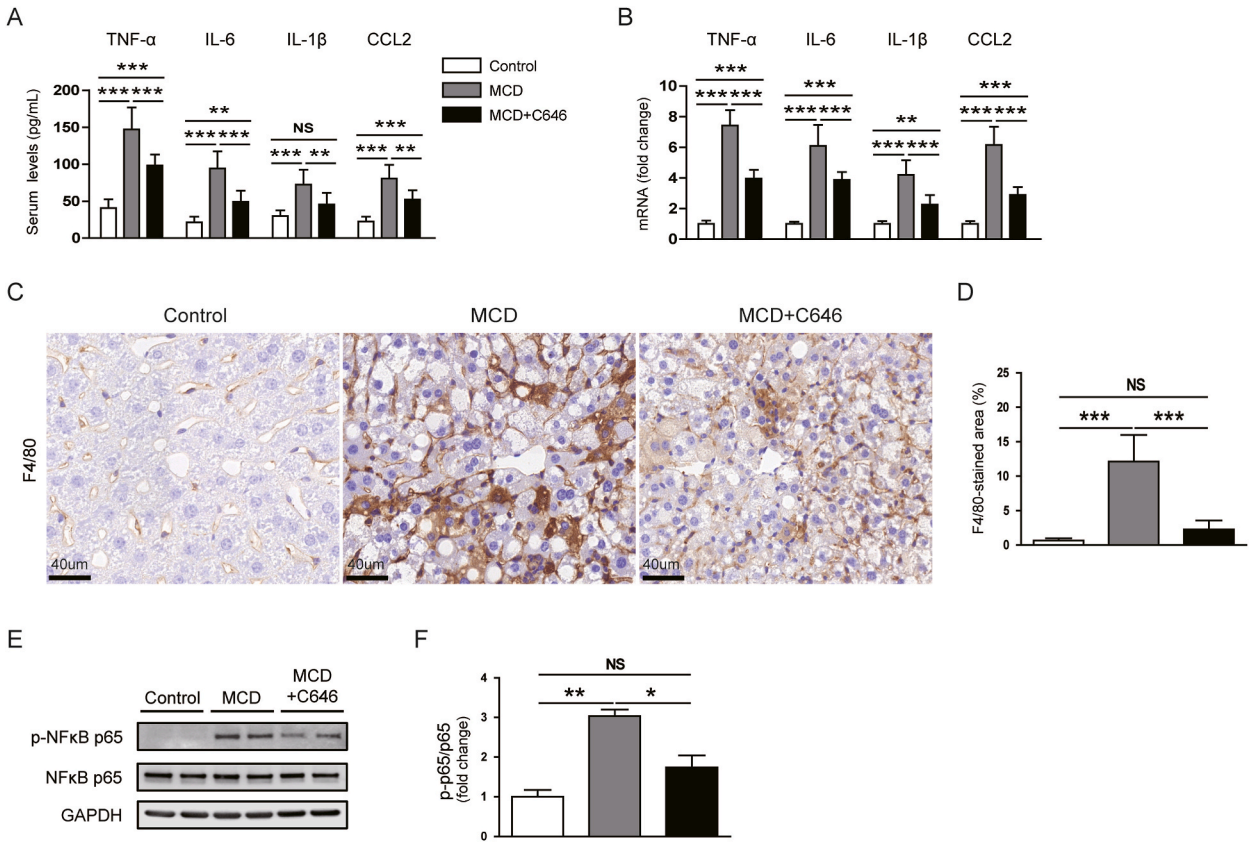

Fig. 5. C646 attenuates inflammation in MCD diet-fed mice. (A) Serum levels of TNF-α, IL-6, IL-1β, and CCL2 (one-way ANOVA with Tukey's HSD *post hoc* test, n = 8). (B) mRNA expression of TNF-α, IL-6, IL-1β, and CCL2 in liver tissues (one-way ANOVA with Tukey's HSD *post hoc* test, n = 8). (C) IHC staining of liver tissues for F4/80. Scale bar = 40 μm. (D) Percentage of areas displaying F4/80 staining (one-way ANOVA with Tukey's HSD *post hoc* test, n = 8). (E) Western blots depicting p-NFκB p65 in liver tissues. The uncropped versions of Western blots are shown in Supplementary of Original Images for Blots. (F) Quantitative analysis of Western blot data (Kruskal-Wallis test with Dunn's *post hoc* test, n = 6). Data are expressed as the mean ± SD. $*p < 0.05$, $**p < 0.01$ and $***p < 0.001$. NS, not significant.

including DNA methylation, histone modifications, and non-coding RNAs, which impact the expression of genes without altering the DNA sequence itself [4,5].

One key epigenetic modification in NASH is the acetylation of histone proteins, particularly influenced by enzymes like p300, a histone acetyltransferase [8–10]. The activity of p300 alters the structure of chromatin, influencing the accessibility of transcription factors to DNA and thereby regulating the transcription of numerous genes involved in lipid metabolism, inflammation, and fibrosis, which are the core features of NASH [13–15]. For instance, abnormal acetylation patterns can lead to increased expression of genes promoting lipid synthesis and accumulation in hepatocytes, triggering steatosis [22]. Concurrently, genes involved in pro-inflammatory pathways may be upregulated, further exacerbating liver damage and fibrosis [23,24]. Thus, the initial steps in the pathogenesis of NASH can be traced back to the modulation of gene expression, orchestrated through complex epigenetic modifications. By influencing these foundational gene regulatory mechanisms, potential therapies, such as the inhibition of enzymes like p300, may be considered promising ways to address the root causes of NASH. In this study, we demonstrated that mice subjected to the MCD diet for 4 weeks exhibited elevated NAFLD activity scores upon histological examination and increased serum levels of AST and ALT. Administration of the p300 inhibitor C646 significantly mitigated NASH evoked by the MCD diet, all while having no discernible impact on changes of body weight and liver weight. Moreover, mice on the MCD diet exhibited heightened p300 expression and increased acetylation of Lys18 and Lys9 on histone H3, both of which are well-known targets of p300 [11], hinting at the potential involvement of p300 in NASH pathogenesis. Treatment with C646 effectively curtailed p300 expression and p300-mediated histone acetylation in MCD diet-fed mice, suggesting that p300 inhibition ameliorates MCD diet-evoked NASH by modulating histone acetylation.

Regarding the utilization of the MCD diet in our experimental model, we recognize its effectiveness in rapidly inducing features characteristic of NASH. However, it is important to address the limitation of significant weight loss observed in animals on this diet. This weight loss is largely attributed to the diet's lack of essential nutrients, specifically methionine and choline. Their deficiency causes a hypermetabolic state in mice, which reduces the efficiency of energy extraction from nutrients, contributing to weight loss [16]. While the MCD diet efficiently models certain aspects of NASH, particularly liver injury and fibrosis, its divergence from typical

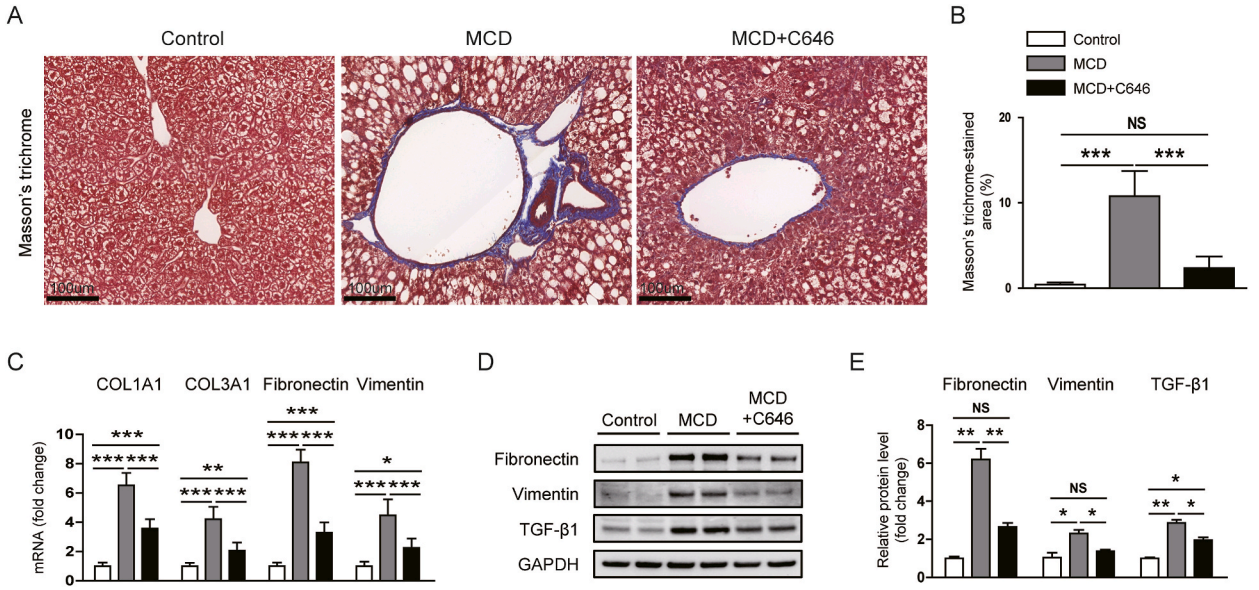

Fig. 6. C646 alleviates fibrosis in MCD diet-fed mice. (A) Masson's trichrome staining of liver tissues. Scale bar = 100 μm. (B) Percentage of areas displaying Masson's trichrome staining (one-way ANOVA with Tukey's HSD *post hoc* test, n = 8). (C) mRNA expression of COL1A1, COL3A1, fibronectin, and vimentin in liver tissues (one-way ANOVA with Tukey's HSD *post hoc* test, n = 8). (D) Western blots depicting fibronectin, vimentin, and TGF-β1 in liver tissues. The uncropped versions of Western blots are shown in Supplementary of Original Images for Blots. (E) Quantitative analysis of Western blot data (Kruskal-Wallis test with Dunn's *post hoc* test, n = 6). Data are expressed as the mean ± SD. $*p < 0.05$, $**p < 0.01$ and $***p < 0.001$. NS, not significant.

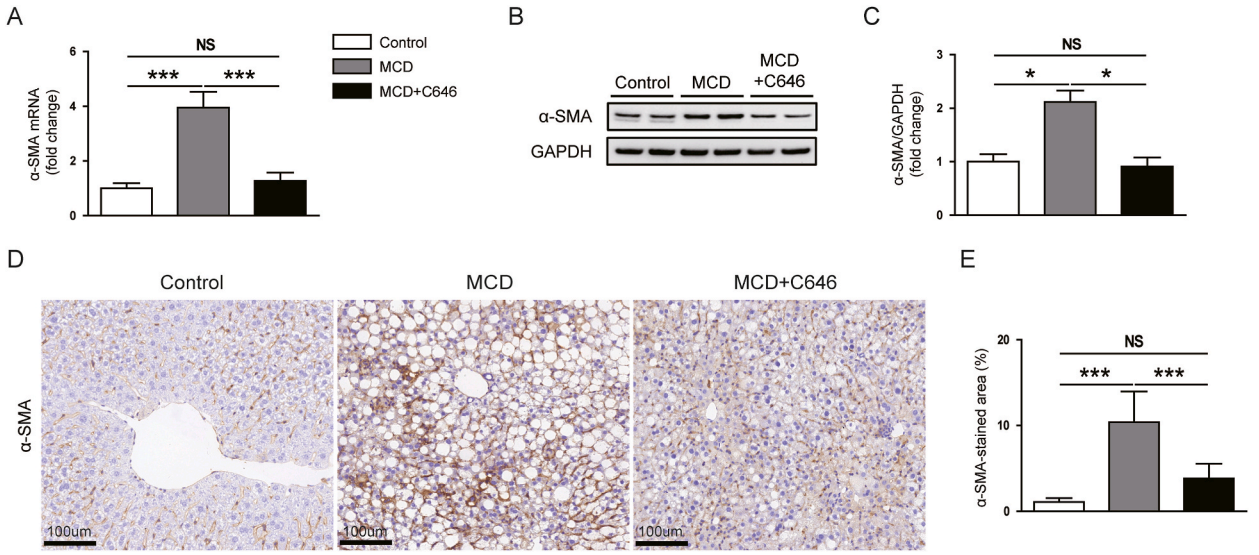

Fig. 7. C646 prevents myofibroblast accumulation in MCD diet-fed mice. (A) mRNA expression of α-SMA in liver tissues (one-way ANOVA with Tukey's HSD *post hoc* test, n = 8). (B) Western blots depicting α-SMA in liver tissues. The uncropped versions of Western blots are shown in Supplementary of Original Images for Blots. (C) Quantitative analysis of Western blot data (Kruskal-Wallis test with Dunn's *post hoc* test, n = 6). (D) IHC staining of liver tissues for α-SMA. Scale bar = 100 μm. (E) Percentage of areas displaying α-SMA staining (one-way ANOVA with Tukey's HSD *post hoc* test, n = 8). Data are expressed as the mean ± SD. $*p < 0.05$ and $***p < 0.001$. NS, not significant.

human NASH conditions, often associated with obesity and metabolic syndrome, should be carefully considered by researchers [17]. The choice of an animal model should align with the specific objectives of the study and the aspects of NASH pathology being investigated. While the MCD diet provides valuable insights, researchers should be aware of its limitations and consider other models that may better represent the human condition of NASH, especially for studies with a strong translational focus.

Excessive hepatic de novo lipogenesis (DNL) contributes to the accumulation of hepatic TG in NASH, making it a prospective target

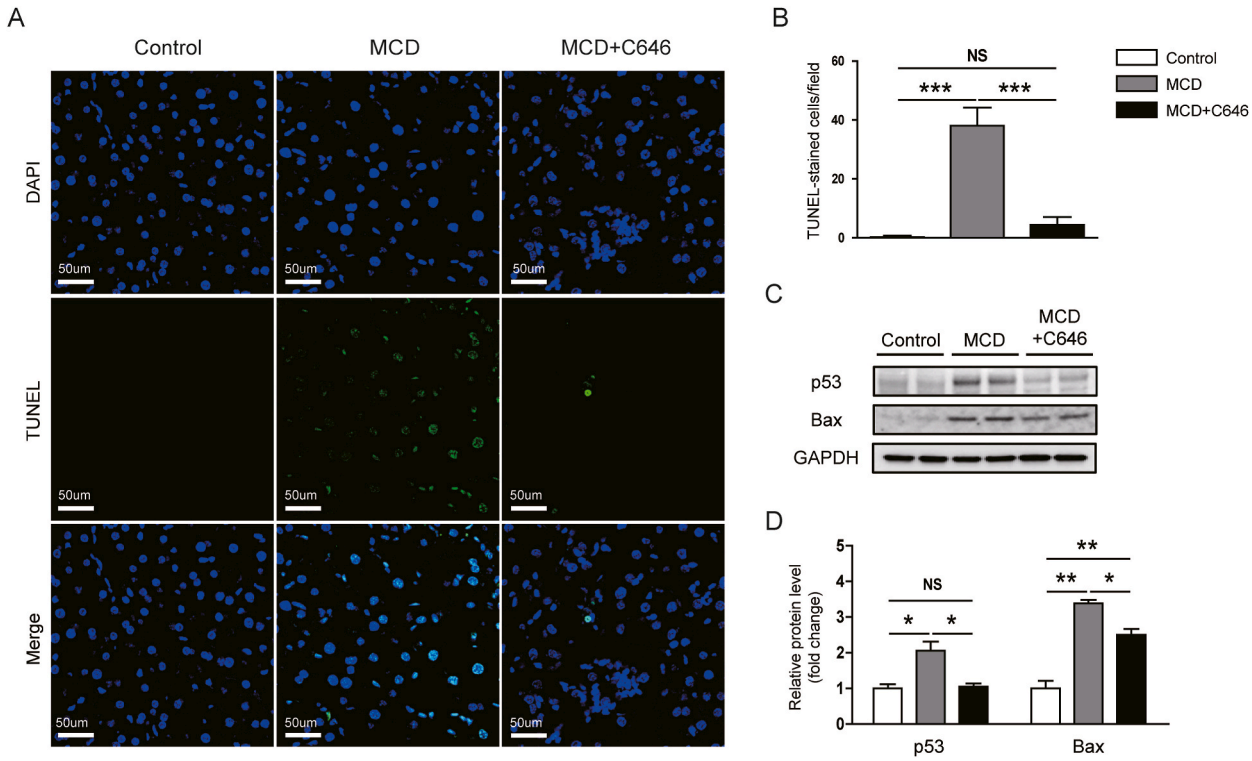

Fig. 8. C646 inhibits apoptosis in MCD diet-fed mice. (A) TUNEL assay on liver tissues. Nuclei were counterstained with DAPI. Scale bar = 50 μm. (B) Number of TUNEL-stained cells (one-way ANOVA with Tukey's HSD *post hoc* test, n = 8). (C) Western blots depicting p53 and Bax expression in liver tissues. The uncropped versions of Western blots are shown in Supplementary of Original Images for Blots. (D) Quantitative analysis of Western blot data (Kruskal-Wallis test with Dunn's *post hoc* test, n = 6). Data are expressed as the mean ± SD. $*p < 0.05$, $**p < 0.01$ and $***p < 0.001$. NS, not significant.

for therapeutic intervention [25]. Our observations revealed that mice exposed to the MCD diet exhibited elevated hepatic TG accumulation alongside the upregulation of DNL-related genes. Notably, SREBP-1c and ChREBP serve as major transcription factors that bolster hepatic DNL in NASH by enhancing the expression of lipogenic genes [2]. C646 treatment was found to inhibit hepatic TG accumulation and reduced the mRNA levels of SREBP-1c, ACC1, FASN, and ChREBP in MCD diet-fed mice, suggesting that p300 inhibition alleviates hepatic TG accumulation, presumably through the modulation of hepatic DNL in MCD diet-induced NASH. Furthermore, p300 inhibition effectively curtailed cytokine production and macrophage infiltration in MCD diet-fed mice. Prior studies have shown that liver-resident macrophages (Kupffer cells) and infiltrating macrophages release pro-inflammatory cytokines, driving the transition from simple steatosis to NASH [26]. In alignment with these findings, p300 inhibition thwarted NFκB activation, as evidenced by the reduced phosphorylation of NFκB p65. NFκB plays a pivotal role in regulating macrophage function and cytokine production, and sustained activation of the NFκB pathway has been observed in animal models of NASH [27] and in NASH patients [28]. Besides addressing steatosis and inflammation, p300 inhibition was shown to alleviate fibrotic changes in MCD diet-fed mice, evident from reduced staining of collagen fibers in Masson's trichrome staining and diminished production of extracellular matrix proteins. Moreover, accumulation of α-SMA-positive myofibroblasts was attenuated by C646 treatment. Myofibroblasts are specialized contractile fibroblasts known for their secretion of substantial amounts of extracellular matrix proteins and inflammatory mediators [29]. Accumulating evidence suggests that hepatic stellate cells (HSCs) are the primary source of myofibroblasts [30], and previous studies have reported significant activation and accumulation of HSCs in MCD diet-fed mice [31,32]. Upon liver injury, HSCs transdifferentiate into myofibroblasts, secreting copious amounts of extracellular matrix proteins, pro-inflammatory cytokines, and profibrogenic mediators, driving liver fibrosis [30].

Hepatocyte apoptosis has garnered attention for its role in the pathophysiology of NASH [33,34], prompting our investigation into the effects of p300 inhibition on apoptosis. In this study, C646 treatment significantly curtailed apoptosis in mice exposed to the MCD diet, as confirmed by TUNEL staining. The expression of p53 and Bax proteins was also reduced by C646. p53 is a transcription factor capable of activating the apoptotic pathway by upregulating pro-apoptotic proteins like Bax [35]. A prior study reported that p53 deficiency reduced the number of apoptotic hepatocytes and mitigated NASH progression in MCD diet-fed mice [36]. Elevated hepatic p53 expression was observed in NASH patients [36], and Witek et al. demonstrated that administration of a pan-caspase inhibitor alleviated fibrosis in MCD diet-fed rodent [37]. These results imply that the anti-apoptotic effect of p300 inhibition contributes to its hepatoprotective action in NASH.

Ferroptosis, an iron-dependent oxidative cell death process, has recently emerged as a focal point of interest due to its integral role

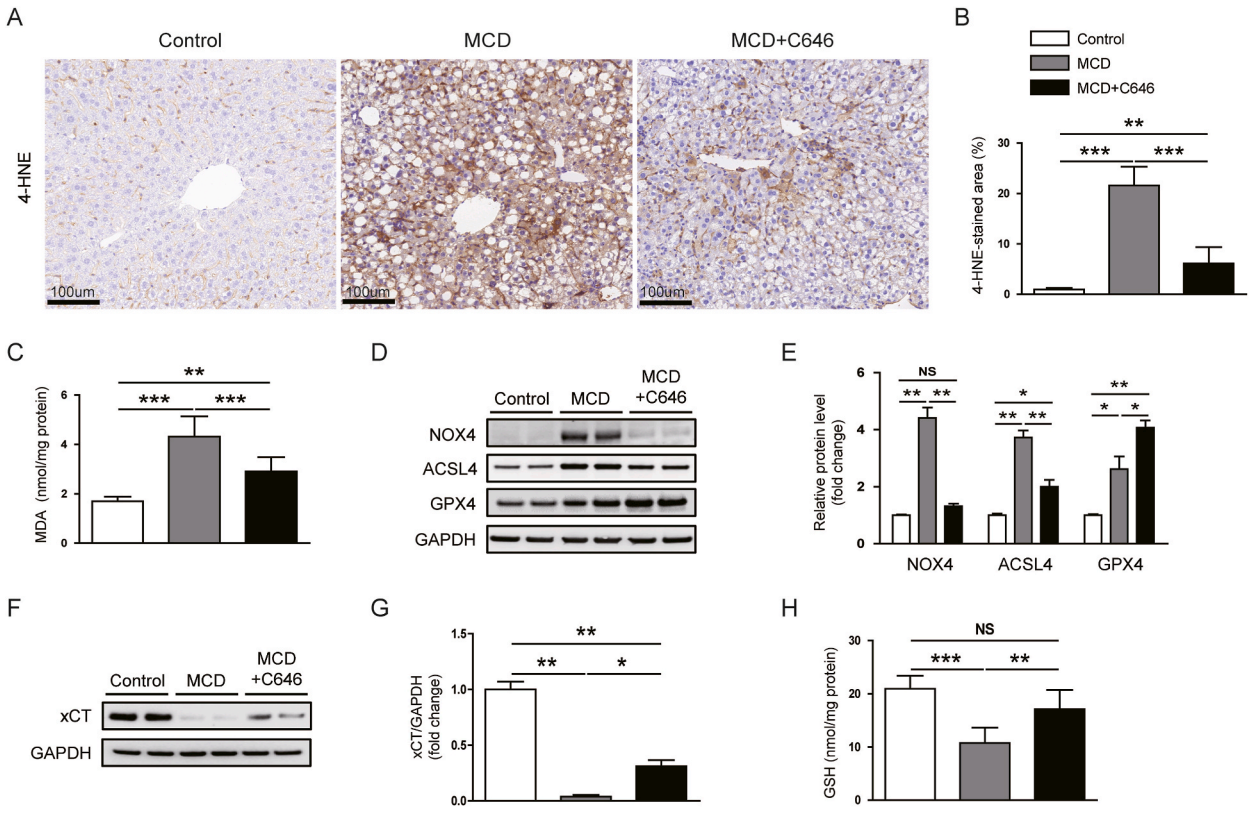

Fig. 9. C646 prevents ferroptosis in MCD diet-fed mice. (A) IHC staining of liver tissues for 4-HNE. Scale bar = 100 μm. (B) Percentage of areas displaying 4-HNE staining (one-way ANOVA with Tukey's HSD *post hoc* test, n = 8). (C) Hepatic MDA levels (one-way ANOVA with Tukey's HSD *post hoc* test, n = 8). (D) Western blots depicting NOX4, ACSL4, and GPX4 in liver tissues. The uncropped versions of Western blots are shown in Supplementary of Original Images for Blots. (E) Quantitative analysis of Western blot data (Kruskal-Wallis test with Dunn's *post hoc* test, n = 6). (F) Western blots depicting xCT in liver tissues. (G) Quantitative analysis of Western blot data (Kruskal-Wallis test with Dunn's *post hoc* test, n = 6). The uncropped versions of Western blots are shown in Supplementary of Original Images for Blots. (H) Hepatic GSH levels (one-way ANOVA with Tukey's HSD *post hoc* test, n = 8). Data are expressed as the mean ± SD. $^{*}p < 0.05$, $^{**}p < 0.01$ and $^{***}p < 0.001$. NS, not significant.

in the pathophysiology of NASH [38,39]. In our study, C646 effectively curtailed lipid peroxidation, a hallmark of ferroptosis, as evidenced by reduced levels of 4-HNE and MDA. MCD diet-fed mice also exhibited elevated expression of NOX4, ACSL4, and GPX4 in the liver. Interestingly, p300 inhibition reduced NOX4 and ACSL4 expression, while enhancing GPX4 expression. NOX4 represents a major enzyme responsible for reactive oxygen species (ROS) production in the liver [40], and recent studies have highlighted the role of NOX4-mediated ROS production in promoting lipid peroxidation in ferroptosis [41,42]. Bettaieb et al. demonstrated that hepatic NOX4 expression is upregulated in animal models of NASH and in NASH patients [43]. Hepatocyte-specific knockout of NOX4 and pharmacological NOX4 inhibition were found to mitigate lipid peroxidation, inflammation, and fibrosis in NASH mice [43]. ACSL4 is an enzyme responsible for the biosynthesis of polyunsaturated fatty acid-containing phospholipids and contributes to lipid peroxidation in ferroptosis [38,39]. Duan et al. reported that genetic and pharmacological ACSL4 inhibition attenuated NASH in mice [44]. On the other hand, GPX4 serves as an antioxidant enzyme that inhibits lipid peroxidation and is recognized as a negative regulator of ferroptosis [38,39]. In line with our results, multiple investigations have indicated the upregulation of GPX4 in mice subjected to the MCD diet [45,46], and a recent study demonstrated that GPX4 activation ameliorated the severity of NASH [47]. Therefore, the increase in GPX4 expression in mice subjected to the MCD diet appears to be an adaptive response to liver injury. GPX4 utilizes GSH to inhibit lipid peroxidation and shield cells against ferroptosis [38,39]. The cystine/glutamate antiporter xCT mediates the uptake of extracellular cystine for GSH biosynthesis [38,39]. Notably, the inhibition of p300 induced upregulation of xCT, accompanied by a restoration of GSH levels in mice subjected to the MCD diet. Altogether, our data indicate that p300 inhibition effectively suppresses ferroptosis in MCD diet-fed mice.

The ER is a pivotal intracellular organelle responsible for the folding and quality control of newly synthesized proteins. When the equilibrium between protein load and the ER's folding capacity is disrupted, misfolded proteins accumulate within the ER, instigating ER stress [48]. ER stress activates the unfolded protein response (UPR), a compensatory process aimed at restoring ER homeostasis. The UPR commences by triggering three ER-localized transmembrane sensors: IRE1, PERK, and ATF6. These UPR pathways work in concert to rebalance ER homeostasis by enhancing chaperone expression, facilitating the degradation of misfolded proteins, and inhibiting protein translation [48]. Numerous studies have underlined the pivotal role of ER stress in the pathogenesis of various

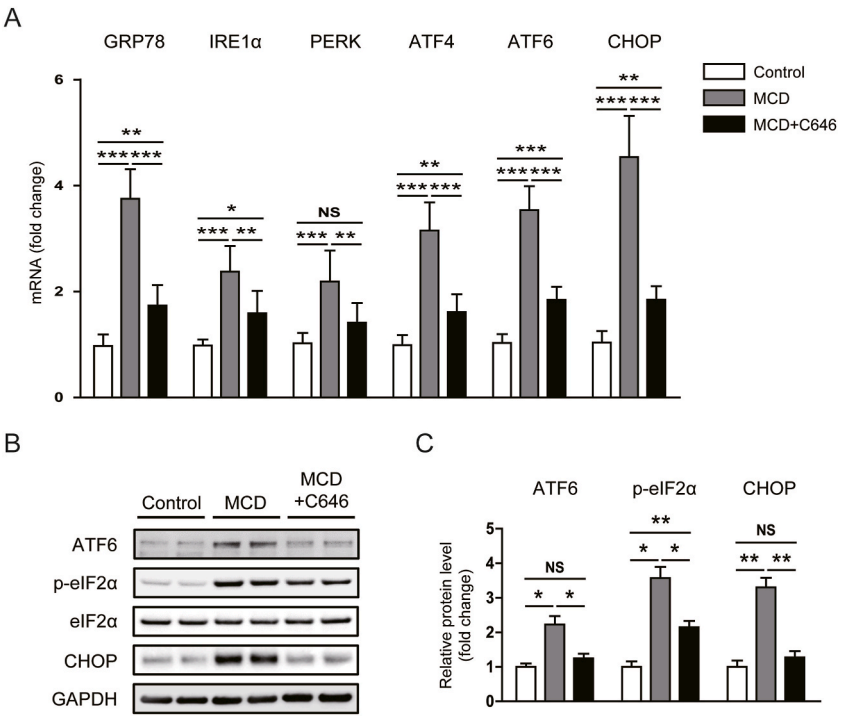

Fig. 10. C646 suppresses ER stress in MCD diet-fed mice. (A) mRNA expression of GRP78, IRE1α, PERK, ATF4, ATF6, and CHOP in liver tissues (one-way ANOVA with Tukey's HSD *post hoc* test, n = 8). (B) Western blots depicting ATF4, p-eIF2α, and CHOP in liver tissues. The uncropped versions of Western blots are shown in Supplementary of Original Images for Blots. (C) Quantitative analysis of Western blot data (Kruskal-Wallis test with Dunn's *post hoc* test, n = 6). Data are expressed as the mean ± SD. $^{*}p < 0.05$, $^{**}p < 0.01$ and $^{***}p < 0.001$. NS, not significant.

diseases, including NASH [48,49]. Accumulating evidence underscores the close association between ER stress and hepatic lipid metabolism, inflammation, fibrosis, and even programmed cell death [48,49]. Therefore, ER stress emerges as a promising therapeutic target for NASH. In this study, p300 inhibition mitigated ER stress, coinciding with the amelioration of NASH, in MCD diet-fed mice, as evidenced by the reduced expression of UPR signaling molecules. In line with our results, prior studies have highlighted that aberrant activation of p300 contributes to hepatic lipid accumulation, inflammation, and fibrosis in liver diseases, primarily by modulating histone acetylation [13–15]. In addition to its role in histone acetylation, p300 can directly bind to and acetylate non-histone proteins such as NFκB and p53 [50,51]. Acetylation exerts multifaceted effects on non-histone proteins through various mechanisms, including the alteration of protein-protein interactions, protein stability, enzymatic activity, and subcellular localization [52]. Increasing evidence suggests that the histone acetyl-transferase activity of p300 is involved in the modulation of ER stress, potentially through the acetylation of histones or UPR signaling molecules [53,54]. It can impact the activation or inhibition of key UPR signaling molecules, leading to a dynamic response to ER stress. Collectively, p300 inhibition effectively suppresses ER stress, thereby ameliorating hepatic lipid accumulation, inflammation, fibrosis, and programmed cell death.

Our study, which focuses on the pharmacological inhibition of p300 in a mouse model of NASH, presents several limitations. First, although the MCD diet model effectively induces symptoms similar to NASH, it may not fully capture the complex pathophysiology of human NASH [16,17]. There are also concerns about the direct applicability of these findings from animal models to humans, given the differences in metabolism and disease progression. Moreover, by concentrating on specific biochemical pathways and markers, our study might not cover the full spectrum of NASH's multifaceted nature. Furthermore, it's important to recognize that our study utilized C646 primarily as a preventive intervention, rather than as a treatment post-onset of NASH. This approach underscores the imperative for subsequent research to investigate the effects of this inhibitor following the establishment of NASH. Such exploration is crucial to better understand the potential therapeutic role of C646 in reversing NASH once it has developed. This area of research could greatly enhance the translational relevance of our findings, offering deeper insights into the therapeutic applications of C646 in clinical settings. Finally, it is crucial to examine the impact of genetic deficiency of p300 in the context of NASH, to gain a deeper understanding of its role and potential as a therapeutic target.

5. Conclusion

The findings presented here underscore the pivotal role of p300 inhibition in alleviating multiple aspects of NASH, particularly in the context of the MCD diet-induced model. By targeting ER stress, p300 inhibition effectively combats hepatic lipid accumulation, suppresses inflammation, mitigates fibrosis, and curtails programmed cell death. The ability of p300 inhibition to comprehensively

address multiple facets of NASH, including its influence on ER stress, suggests a multifaceted approach to tackling this complex and debilitating disease. As we move forward, further research into the specific molecular pathways affected by p300 inhibition and its broader implications in the context of ER stress will be essential. This deeper understanding will empower the development of more targeted and effective therapies for NASH, potentially transforming the landscape of NASH treatment and patient care.

Ethics approval

The animal experiment was approved by the Institutional Animal Care and Use Committee of the Daegu Catholic University Medical Center (DCIAFCR-220628-10-Y).

Funding statement

This study was supported by the Basic Science Research Program through the National Research Foundation of Korea (NRF), funded by the Ministry of Science, ICT, and Future Planning (NRF-2022R1G1A1007988 and NRF-2023R1A2C1006384) and the Ministry of Education (RS-2023-00243420).

Data availability statement

The data that supports the findings of this study are available within the article.

CRediT authorship contribution statement

Jung-Yeon Kim: Writing – original draft, Investigation, Funding acquisition, Formal analysis, Conceptualization. **Ah Young Yang:** Writing – original draft, Investigation, Formal analysis, Conceptualization. **Kiryeong Kim:** Investigation. **Hyun Hee Kwon:** Writing – review & editing, Resources, Formal analysis. **Jaechan Leem:** Writing – review & editing, Project administration, Funding acquisition, Conceptualization. **Yun-A Kim:** Writing – review & editing, Supervision, Funding acquisition, Conceptualization.

Declaration of competing interest

The authors declare the following financial interests/personal relationships which may be considered as potential competing interests:Jaechan Leem reports financial support was provided by the National Research Foundation of Korea (NRF). Yun-A Kim reports financial support was provided by the National Research Foundation of Korea (NRF). Jung-Yeon Kim reports financial support was provided by the National Research Foundation of Korea (NRF). If there are other authors, they declare that they have no known competing financial interests or personal relationships that could have appeared to influence the work reported in this paper.

Appendix A. Supplementary data

Supplementary data to this article can be found online at https://doi.org/10.1016/j.heliyon.2024.e30908.

References

[1] E.E. Powell, V.W. Wong, M. Rinella, Non-alcoholic fatty liver disease, Lancet 397 (2021) 2212–2224.
[2] E. Buzzetti, M. Pinzani, E.A. Tsochatzis, The multiple-hit pathogenesis of non-alcoholic fatty liver disease (NAFLD), Metabolism 65 (2016) 1038–1048.
[3] G. Parthasarathy, X. Revelo, H. Malhi, Pathogenesis of nonalcoholic steatohepatitis: an overview, Hepatol. Commun. 4 (2020) 478–492.
[4] J. Lee, Y. Kim, S. Friso, S.W. Choi, Epigenetics in non-alcoholic fatty liver disease, Mol. Aspect. Med. 54 (2017) 78–88.
[5] S. Guha, S. Sesili, I.H. Mir, C. Thirunavukkarasu, Epigenetics and mitochondrial dysfunction insights into the impact of the progression of non-alcoholic fatty liver disease, Cell Biochem. Funct. 41 (2023) 4–19.
[6] Z. Herceg, Epigenetic mechanisms as an interface between the environment and genome, Adv. Exp. Med. Biol. 903 (2016) 3–15.
[7] X. An, X. Lan, Z. Feng, X. Li, Q. Su, Histone modification: biomarkers and potential therapies in colorectal cancer, Ann. Hum. Genet. 87 (2023) 274–284.
[8] Q. Chen, B. Yang, X. Liu, X.D. Zhang, L. Zhang, T. Liu, Histone acetyltransferases CBP/p300 in tumorigenesis and CBP/p300 inhibitors as promising novel anticancer agents, Theranostics 12 (2022) 4935–4948.
[9] L.M. Valor, J. Viosca, J.P. Lopez-Atalaya, A. Barco, Lysine acetyltransferases CBP and p300 as therapeutic targets in cognitive and neurodegenerative disorders, Curr. Pharmaceut. Des. 19 (2013) 5051–5064.
[10] N. Di Pietrantonio, et al., Diabetes and its cardiovascular complications: potential role of the acetyltransferase p300, Cells 12 (3) (2023) 431.
[11] J.Y. Kim, J. Jo, J. Leem, K.K. Park, Inhibition of p300 by garcinol protects against cisplatin-induced acute kidney injury through suppression of oxidative stress, inflammation, and tubular cell death in mice, Antioxidants 9 (2020) 1271.
[12] J. Peng, J. Li, J. Huang, P. Xu, H. Huang, Y. Liu, et al., p300/CBP inhibitor A-485 alleviates acute liver injury by regulating macrophage activation and polarization, Theranostics 9 (2019) 8344–8361.
[13] W. Yao, T. Wang, F. Huang, p300/CBP as a key nutritional sensor for hepatic energy homeostasis and liver fibrosis, BioMed Res. Int. 2018 (2018) 8168791.
[14] F. Zhou, Q. Liu, L. Zhang, Q. Zhu, S. Wang, K. Zhu, et al., Selective inhibition of CBP/p300 HAT by A-485 results in suppression of lipogenesis and hepatic gluconeogenesis, Cell Death Dis. 11 (2020) 745.
[15] H. Kim, S.Y. Park, S.Y. Lee, J.H. Kwon, S. Byun, M.J. Kim, et al., Therapeutic effects of selective p300 histone acetyl-transferase inhibitor on liver fibrosis, BMB Rep 56 (2023) 114–119.

[16] M.V. Machado, G.A. Michelotti, G. Xie, T. Almeida Pereira, J. Boursier, B. Bohnic, et al., Mouse models of diet-induced nonalcoholic steatohepatitis reproduce the heterogeneity of the human disease, PLoS One 10 (2015) e0127991.
[17] K. Stephenson, L. Kennedy, L. Hargrove, J. Demieville, J. Thomson, G. Alpini, et al., Updates on dietary models of nonalcoholic fatty liver disease: current studies and insights, Gene Expr. 18 (2018) 5–17.
[18] S.H. Kim, Y. Lim, J.B. Park, J.H. Kwak, K.J. Kim, J.H. Kim, et al., Comparative study of fatty liver induced by methionine and choline-deficiency in C57BL/6N mice originating from three different sources, Lab Anim Res 33 (2017) 157–164.
[19] A.G. Lazar, M.L. Vlad, A. Manea, M. Simionescu, S.A. Manea, Activated histone acetyltransferase p300/CBP-related signalling pathways mediate up-regulation of NADPH oxidase, inflammation, and fibrosis in diabetic kidney, Antioxidants 10 (2021) 1356.
[20] X. Xu, J. Li, X. Long, S. Tao, X. Yu, X. Ruan, et al., C646 protects against DSS-induced colitis model by targeting NLRP3 inflammasome, Front. Pharmacol. 12 (2021) 707610.
[21] J. Li, X. Deng, T. Bai, S. Wang, Q. Jiang, K. Xu, Resolvin D1 mitigates non-alcoholic steatohepatitis by suppressing the TLR4-MyD88-mediated NF-κB and MAPK pathways and activating the Nrf2 pathway in mice, Int. Immunopharm. 88 (2020) 106961.
[22] G. Assante, S. Chandrasekaran, S. Ng, A. Tourna, C.H. Chung, K.A. Isse, et al., Acetyl-CoA metabolism drives epigenome change and contributes to carcinogenesis risk in fatty liver disease, Genome Med. 14 (2022) 67.
[23] M. Ghizzoni, H.J. Haisma, H. Maarsingh, F.J. Dekker, Histone acetyltransferases are crucial regulators in NF-κB mediated inflammation, Drug Discov, Today Off. 16 (2011) 504–511.
[24] J. Gao, B. Wei, M. Liu, P. Hirsova, T.S. Sehrawat, S. Cao, et al., Endothelial p300 promotes portal hypertension and hepatic fibrosis through C-C motif chemokine ligand 2-mediated angiocrine signaling, Hepatology 73 (2021) 2468–2483.
[25] E.J. Lawitz, K.W. Li, E. Nyangau, T.J. Field, J.C. Chuang, A. Billin, et al., Elevated de novo lipogenesis, slow liver triglyceride turnover, and clinical correlations in nonalcoholic steatohepatitis patients, J. Lipid Res. 63 (2022) 100250.
[26] K. Kazankov, S.M.D. Jørgensen, K.L. Thomsen, H.J. Møller, H. Vilstrup, J. George, et al., The role of macrophages in nonalcoholic fatty liver disease and nonalcoholic steatohepatitis, Nat. Rev. Gastroenterol. Hepatol. 16 (2019) 145–159.
[27] A. Dela Peña, I. Leclercq, J. Field, J. George, B. Jones, G. Farrell, NF-kappaB activation, rather than TNF, mediates hepatic inflammation in a murine dietary model of steatohepatitis, Gastroenterology 129 (2005) 1663–1674.
[28] P.S. Ribeiro, H. Cortez-Pinto, S. Solá, R.E. Castro, R.M. Ramalho, A. Baptista, et al., Hepatocyte apoptosis, expression of death receptors, and activation of NF-kappaB in the liver of nonalcoholic and alcoholic steatohepatitis patients, Am. J. Gastroenterol. 99 (2004) 1708–1717.
[29] C. Bocca, F. Protopapa, B. Foglia, M. Maggiora, S. Cannito, M. Parola, et al., Hepatic myofibroblasts: a heterogeneous and redox-modulated cell population in liver fibrogenesis, Antioxidants 11 (2022) 1278.
[30] T. Tsuchida, S.L. Friedman, Mechanisms of hepatic stellate cell activation, Nat. Rev. Gastroenterol. Hepatol. 14 (2017) 397–411.
[31] K. Tomita, T. Teratani, T. Suzuki, M. Shimizu, H. Sato, K. Narimatsu, et al., Free cholesterol accumulation in hepatic stellate cells: mechanism of liver fibrosis aggravation in nonalcoholic steatohepatitis in mice, Hepatology 59 (2014) 154–169.
[32] X.X. Ni, X.Y. Li, Q. Wang, J. Hua, Regulation of peroxisome proliferator-activated receptor-gamma activity affects the hepatic stellate cell activation and the progression of NASH via TGF-β1/Smad signaling pathway, J. Physiol. Biochem. 77 (2021) 35–45.
[33] A.E. Feldstein, A. Canbay, P. Angulo, M. Taniai, L.J. Burgart, K.D. Lindor, et al., Hepatocyte apoptosis and fas expression are prominent features of human nonalcoholic steatohepatitis, Gastroenterology 125 (2003) 437–443.
[34] R. Gao, H. Tang, J. Mao, Programmed cell death in liver fibrosis, J. Inflamm. Res. 16 (2023) 3897–3910.
[35] H.H. Wu, S. Leng, Y. Abuetabh, C. Sergi, D.D. Eisenstat, R. Leng, The SWIB/MDM2 motif of UBE4B activates the p53 pathway, Mol. Ther. Nucleic Acids 31 (2023) 466–481.
[36] K. Tomita, T. Teratani, T. Suzuki, T. Oshikawa, H. Yokoyama, K. Shimamura, et al., p53/p66Shc-mediated signaling contributes to the progression of non-alcoholic steatohepatitis in humans and mice, J. Hepatol. 57 (2012) 837–843.
[37] R.P. Witek, W.C. Stone, F.G. Karaca, W.K. Syn, T.A. Pereira, K.M. Agboola, et al., Pan-caspase inhibitor VX-166 reduces fibrosis in an animal model of nonalcoholic steatohepatitis, Hepatology 50 (2009) 1421–1430.
[38] H. Zhang, E. Zhang, H. Hu, Role of ferroptosis in non-alcoholic fatty liver disease and its implications for therapeutic strategies, Biomedicines 9 (2021) 1660.
[39] F. Xiong, Q. Zhou, X. Huang, P. Cao, Y. Wang, Ferroptosis plays a novel role in nonalcoholic steatohepatitis pathogenesis, Front. Pharmacol. 13 (2022) 1055793.
[40] D. Matuz-Mares, H. Vázquez-Meza, M.M. Vilchis-Landeros, NOX as a therapeutic target in liver disease, Antioxidants 11 (10) (2022) 2038.
[41] J. Xie, H. Lv, X. Liu, Z. Xia, J. Li, E. Hong, et al., Nox4-and Tf/TfR-mediated peroxidation and iron overload exacerbate neuronal ferroptosis after intracerebral hemorrhage: involvement of EAAT3 dysfunction, Free Radic. Biol. Med. 199 (2023) 67–80.
[42] M.W. Park, H.W. Cha, J. Kim, J.H. Kim, H. Yang, S. Yoon, et al., NOX4 promotes ferroptosis of astrocytes by oxidative stress-induced lipid peroxidation via the impairment of mitochondrial metabolism in Alzheimer's diseases, Redox Biol. 41 (2021) 101947.
[43] A. Bettaieb, J.X. Jiang, Y. Sasaki, T.I. Chao, Z. Kiss, X. Chen, et al., Hepatocyte nicotinamide adenine dinucleotide phosphate reduced oxidase 4 regulates stress signaling, fibrosis, and insulin sensitivity during development of steatohepatitis in mice, Gastroenterology 149 (2015) 468–480.e10.
[44] J. Duan, Z. Wang, R. Duan, C. Yang, R. Zhao, Q. Feng, et al., Therapeutic targeting of hepatic ACSL4 ameliorates NASH in mice, Hepatology 75 (2022) 140–153.
[45] J. Choi, H. Choi, J. Chung, Icariin supplementation suppresses the markers of ferroptosis and attenuates the progression of nonalcoholic steatohepatitis in mice fed a methionine choline-deficient diet, Int. J. Mol. Sci. 25 (2023) 12510.
[46] D. Lu, Q. Xia, Z. Yang, S. Gao, S. Sun, X. Luo, et al., ENO3 promoted the progression of NASH by negatively regulating ferroptosis via elevation of GPX4 expression and lipid accumulation, Ann. Transl. Med. 9 (2021) 661.
[47] J. Qi, J.W. Kim, Z. Zhou, C.W. Lim, B. Kim, Ferroptosis affects the progression of nonalcoholic steatohepatitis via the modulation of lipid peroxidation-mediated cell death in mice, Am. J. Pathol. 190 (2020) 68–81.
[48] A. Ajoolabady, N. Kaplowitz, C. Lebeaupin, G. Kroemer, R.J. Kaufman, H. Malhi, et al., Endoplasmic reticulum stress in liver diseases, Hepatology 77 (2023) 619–639.
[49] C. Lebeaupin, D. Vallée, Y. Hazari, C. Hetz, E. Chevet, B. Bailly-Maitre, Endoplasmic reticulum stress signalling and the pathogenesis of non-alcoholic fatty liver disease, J. Hepatol. 69 (2018) 927–947.
[50] L.F. Chen, Y. Mu, W.C. Greene, Acetylation of RelA at discrete sites regulates distinct nuclear functions of NF-kappaB, EMBO J. 21 (2002) 6539–6548.
[51] W. Gu, R.G. Roeder, Activation of p53 sequence-specific DNA binding by acetylation of the p53 C-terminal domain, Cell 90 (1997) 595–606.
[52] T. Narita, B.T. Weinert, C. Choudhary, Functions and mechanisms of non-histone protein acetylation, Nat. Rev. Mol. Cell Biol. 20 (2019) 156–174.
[53] P. Baumeister, S. Luo, W.C. Skarnes, G. Sui, E. Seto, Y. Shi, et al., Endoplasmic reticulum stress induction of the Grp78/BiP promoter: activating mechanisms mediated by YY1 and its interactive chromatin modifiers, Mol. Cell Biol. 25 (2005) 4529–4540.
[54] J.F. Li, Y.S. Li, Y.Y. Zhang, S.F. Sun, T.S. Han, Y.H. Li, et al., Regulation of P300 and HDAC1 on endoplasmic reticulum stress in isoniazid-induced HL-7702 hepatocyte injury, J. Cell. Physiol. 234 (9) (2019) 15299–15307.